A Novel Approach for State of Health Estimation and Remaining Useful Life Prediction of Supercapacitors Using an Improved Honey Badger Algorithm Assisted Hybrid Neural Network

Zhenxiao Yi, Shi Wang, Zhaoting Li, Licheng Wang, and Kai Wang

***Abstract*—Supercapacitors (SCs) are widely recognized as excellent clean energy storage devices. Accurate state of health (SOH) estimation and remaining useful life (RUL) prediction are essential for ensuring their safe and reliable operation. This paper introduces a novel method for SOH estimation and RUL prediction, based on a hybrid neural network optimized by an improved honey badger algorithm (HBA). The method combines the advantages of convolutional neural network (CNN) and bidirectional long-short-term memory (BiLSTM) neural network. The HBA optimizes the hyperparameters of the hybrid neural network. The CNN automatically extracts deep features from time series data and reduces dimensionality, which are then used as input for the BiLSTM. Additionally, recurrent dropout is introduced in the recurrent layer to reduce overfitting and facilitate the learning process. This approach not only improves the accuracy of estimates and forecasts but also significantly reduces data processing time. SCs under different working conditions are used to validate the proposed method. The results show that the proposed hybrid model effectively extracts features, enriches local details, and enhances global perception capabilities. The proposed hybrid model outperforms single models, reducing the root mean square error to below 1%, and offers higher prediction accuracy and robustness compared to other methods.**

***Index Terms*—Supercapacitors, state of health, remaining useful life, honey badger algorithm, recurrent dropout.**

I. Introduction

As the energy crisis and environmental pollution worsen, supercapacitors are increasingly adopted as new energy storage elements due to their high efficiency, practicality, and environmental friendliness [1], [2]. Compared to conventional capacitors, supercapacitors have faster dynamic responses and larger capacities, enabling quicker charging and discharging [3]–[5]. This capability allows supercapacitors to provide higher power output within a short period. Unlike traditional batteries, supercapacitors offer high power density, fast charging and discharging, a wide operating temperature range, and a long service life [6], [7]. In hybrid energy storage systems, they are typically connected in series and parallel with batteries to reduce electrical stress fluctuations on the battery load, and to increase the voltage and current of the energy storage system [8], [9]. This configuration also enhances the overall energy efficiency of the energy storage system [10], [11]. However, due to microscopic differences in monomer structure parameters and application conditions, the service life of different supercapacitors varies significantly. This can lead to problems such as uneven temperature distribution and voltage imbalance in hybrid energy storage systems [12], [13]. These issues further affect the aging process of supercapacitors, compromising the safety and reliability of the entire system.

Received: December 25, 2023
Accepted: June 5, 2024
Published Online: November 1, 2024

Zhenxiao Yi is with the School of Electrical Engineering, Qingdao University, Qingdao 266071, China, and the State Key Laboratory of Reliability and Intelligence of Electrical Equipment, Hebei University of Technology, Tianjin 300130, China (e-mail: yzx@qdu.edu.cn).

Shi Wang (corresponding author) is with the Key Laboratory of Intelligent Information Processing, Institute of Computing Technology, Chinese Academy of Sciences, Beijing 100190, China (e-mail: wangshi@ict.ac.cn).

Zhaoting Li is with the School of Engineering, Brown University, Providence, Rhode Island 02912, USA (e-mail: zhaoting_li@brown.edu).

Licheng Wang is with the School of Information Engineering, Zhejiang University of Technology, Hangzhou 310014, China (e-mail: wanglicheng@zjut.edu.cn).

Kai Wang (corresponding author) is with the School of Electrical Engineering, Qingdao University, Qingdao 266071, China (e-mail: wkwj888@163.com).

DOI: 10.23919/PCMP.2023.000187

Accurately estimating the health status and predicting the remaining service life of supercapacitors constitute a critical area of research in supercapacitor technology [14]. These assessments are vital for developing maintenance and replacement plans and provide a reliable reference for preventing related accidents [15]–[17]. Therefore, accurate state of health (SOH) estimation and remaining useful life (RUL) prediction for supercapacitors are essential.

SOH is a key indicator for evaluating the life of supercapacitors, representing their aging state from the beginning of life to the end of life (EOL) [18]–[20]. SOH is typically defined as the ratio of the current maximum capacity to the rated capacity of a supercapacitor. This study adopts the same definition for SOH. When its value falls below 80%, the supercapacitor is considered to have reached the EOL [21]–[23]. This threshold is also known as the supercapacitor lifetime failure threshold. Due to the phenomenon of capacity regeneration during the aging process of supercapacitors, evaluating their health condition solely based on SOH can lead to discrepancies, as supercapacitors may have the same remaining usable capacity and SOH but different points of RUL. Capacity regeneration can extend the lifespan of supercapacitors to some extent but does not imply a full restoration to their previous health level corresponding to the same SOH [24]–[27]. Therefore, relying solely on SOH for health assessment is insufficient for obtaining a comprehensive and accurate evaluation. Integrating the current SOH and RUL of supercapacitors is necessary for a thorough diagnosis. However, commonly used methods often estimate only one of these indicators [28]–[31]. Thus, as a complement to SOH, this paper aims to predict RUL alongside SOH. RUL typically refers to the remaining number of charge and discharge cycles from the current state to EOL [32]. To predict RUL, the attenuation model is generally established based on capacity data from supercapacitor aging experiments. There are currently two primary approaches to this: model-based and data-driven.

The model-based approach is primarily defined by the internal aging mechanisms of the supercapacitor and the identification of parameters used to characterize its operation. Currently, the dominant approaches include the Kalman filter (KF) and its derived algorithms. For example, in [33], the extended Kalman filter (EKF) and the multiscale hybrid Kalman filter are used to estimate SOH. Similarly, in [34], an ensemble Kalman filter (EnKF) is employed to estimate the internal state of a Li-ion battery, yielding favorable results. In [35], particle filter (PF) algorithms are used to predict the RUL of supercapacitors with high accuracy based on aging conditions, as well as capacitance and resistance thresholds. Another study employs a multiscale extended Kalman filter and Gauss-Hermite particle filter to update the in-situ parameters of the capacity degradation model for final RUL prediction [36]. However, due to the complex internal characteristics of supercapacitors, such models often involve numerous mathematical equations and parametric variables, leading to drawbacks such as complicated computational processes and difficulty in accounting for environmental factors. Additionally, designing accelerated aging tests to collect effective offline training data is challenging, making these models difficult to apply effectively in practice.

Data-driven approaches, particularly those based on neural networks, are currently a hot research topic [37]. These approaches offer advantages such as adaptability, flexibility, and speed, without requiring complex mechanisms. Among them, recurrent neural networks (RNNs), which use hidden neurons to add recurrent connections to effectively extract and update temporal data relevance, becoming an effective means of processing such data [38]–[40]. However, simple RNNs suffer from the disadvantages of gradient vanishing and gradient explosion, making them less practical for tasks involving extended temporal dependencies. To address these issues, the long short-term memory (LSTM) neural network incorporates additional interactions within each module (or unit), thereby overcoming limitations related to temporal dependencies. Reference [41] uses enhanced LSTM to estimate the SOH of lithium-ion batteries, demonstrating good robustness and estimation accuracy. Reference [42] proposes a data-driven method based on a stochastic partial charging process and sparse Gaussian process regression (GPR), achieving high accuracy under three different types of battery data. This method also shows the highest accuracy and reliability compared with other methods and is more suitable for practical applications. Reference [43] combines a fully connected layer and LSTM to accurately and efficiently estimate SOH, leveraging the complementary strengths of multiple algorithms for improved results. Furthermore, the integration of LSTM networks with other methods has been shown to enhance estimation accuracy. Reference [44] proposes a battery capacity prediction method based on charging data and data-driven algorithms, which can effectively reduce the limitations of battery management systems in measurement and computing capabilities. A sequence-to-sequence model is used to predict future capacity trajectories and two residual models based on GPR are proposed to compensate for prediction errors caused by local capacity changes, achieving an error below 1.6% in predicting the remaining capacity sequence. Reference [45] proposes a deep learning integration method based on Bayesian model averaging (BMA) and LSTM to predict the RUL of lithium-ion batteries. The online iterative training strategy of the BMA algorithm is introduced to achieve superior prediction performance compared to offline training strategies. Furthermore, some studies use the bidirectional long-short-term memory (BiLSTM) model

to enable the output layer to receive time series information from backward and forward, and the results show that the BiLSTM model provides a higher prediction accuracy. Reference [46] uses BiLSTM to establish a data-based model to predict supercapacitor RUL. By adding reverse recurrent layers, the capacity space is increased, and the prediction error is reduced. In the feature extraction stage, the one-dimensional convolutional neural network (1D-CNN) model is used to automatically extract features based on the characteristics of the sequence data, which can capture more detailed information with minimal manual intervention, making it a current research hotspot. However, when dealing with long sequence data, CNN cannot capture the dependencies between sequence information. Therefore, to address this shortcoming, it generally needs to be used with other neural networks. Reference [47] proposes a hybrid CNN-LSTM model to realize the prediction of battery RUL, which has excellent performance. Reference [48] realizes the estimation of battery SOH by constructing a CNN-LSTM fusion neural network and combining it with a gated recurrent unit (GRU). Compared with traditional single models, the proposed combination model has higher estimation accuracy. However, due to the simplified structure of GRU, its performance in handling long time series data such as those from supercapacitors, is not as good as LSTM. Furthermore, the combined model may face issues such as high computational complexity, complex structure, and difficulty in manual tuning. To sum up, LSTM is effective for learning long-term dependencies, while CNN can capture local and global correspondences, playing a crucial role in feature mapping. Since LSTM can only capture the unidirectional long-term and short-term characteristics of the input data, the BiLSTM model integrates forward and backward information, is more advantageous for long-term series data.

However, most of the current algorithms are mainly applied to lithium batteries. Due to the differences in structure, composition, working principle, and application conditions of supercapacitors, some methods exhibit poor prediction accuracy or applicability when used on supercapacitors. To address the limitations that CNN and LSTM models can only capture local features and unidirectional long-term and short-term features, this paper combines the advantages of 1D-CNN and BiLSTM models, and innovatively proposes an improved CNN-BiLSTM hybrid model. Using improved honey badger algorithm (HBA) to optimize the model overcomes the problems of high mathematical complexity, strong model dependence, difficult parameter optimization, and low precision present in existing methods. While improving the estimation and prediction accuracy, the time required for data processing is also greatly reduced. Therefore, the model can flexibly and robustly extract the long-term and short-term features from complex data sets and the characteristics of time series data.

The contributions to this research can be summarized as follows.

1) The 1D-CNN demonstrates powerful feature extraction capabilities, excelling at gathering local variables through convolutional operations and preserving all local clues as feature maps. By leveraging bidirectional information flow, BiLSTM captures correlations and long-term dependencies in sequences comprehensively. Therefore, the proposed model retains the structural and generalization advantages of both 1D-CNN and BiLSTM, enabling accurate and fast estimation and prediction of SOH and RUL for supercapacitors. The experimental results indicate significant potential of this approach.

2) Introducing recurrent dropout and applying dropout in the recurrent layers reduce overfitting, thereby facilitating the learning process.

3) By incorporating opposition-based learning (OBL), the honey badger optimization algorithm has been enhanced to possess a powerful global search capability, aiding in the discovery of the global optimal solution. By simulating adaptive behaviors observed during foraging processes, automatic adjustment of algorithm parameters is achieved. As a result, the proposed method exhibits higher robustness and scalability.

4) The proposed hybrid model effectively leverages information present in observational data, making it applicable to supercapacitors under various operating conditions and demonstrating good generalization abilities. Additionally, this method may provide valuable reference for health estimation of lithium-ion batteries.

In this research, an innovative neural network architecture called HBA-CNN-BiLSTM is proposed. By combining local features based on 1D-CNN with global variables from the BiLSTM model and utilizing the advanced improved HBA intelligent optimization algorithm to optimize and adjust the network's hyperparameters, precise estimation and prediction of SOH and RUL for supercapacitors operating under different conditions are achieved.

The rest of the paper is organized as follows. Section II clarifies the rationale and structure of supercapacitor SOH estimation and RUL models. In Section III, the supercapacitor aging test platform and its aging factors are introduced. Section IV presents the experimental results and error analysis for SOH estimation and RUL prediction. Section V presents the conclusion.

II. METHODOLOGIES

This section examines the proposed methods for SOH estimation and RUL prediction for supercapacitors. The proposed HBA-CNN-BiLSTM model is introduced in detail. The main idea of this method is to use the HBA algorithm to optimize the hyperparameters of the

CNN-BiLSTM structure. Combining the advantages of 1D-CNN and BiLSTM, recurrent dropout is used to prevent overfitting and improve the stability and learning efficiency of the network. It is worth noting that the proposed model is the first attempt at the application of SOH estimation and RUL prediction of supercapacitors.

A. One Dimensional Convolutional Neural Network

CNN has an excellent ability to process multidimensional data and has gained wide attention in the fields of image recognition, natural language processing, and time series classification [49], [50]. CNN with different dimensions is used to process different data to obtain better results [51]. Among them, 1D-CNN has outstanding performance in processing one-dimensional time series data [52]–[54]. Since the experimental data of the supercapacitor is one-dimensional time series data, it is a reasonable choice to use 1D-CNN to extract and learn the relevant features in the input data. Based on the characteristic that the data has intrinsic dependence between adjacent dimensions, 1D-CNN can use shared convolutional filters to extract the identification features of the data. Complex feature representations are extracted from the data using a convolutional layer in 1D-CNN, a pooling layer is used to achieve dimensionality reduction while maintaining relevant features, and a fully connected layer is used to obtain prediction results [55]–[57]. The activation function is rectified linear unit (ReLU), which is resilient to the gradient vanishing problem and can improve the trainability of the network [58]. Among others, the use of local connectivity, shared weights, pooling, and multilayers constitute the key to the success of 1D-CNN.

The 1D-CNN module is the first component of the proposed HBA-CNN-BiLSTM architecture. The designed 1D-CNN consists of a one-dimensional convolutional layer, batch normalization layer, ReLU layer, pooling layer, and a flatten layer. The convolutional layer extracts hidden information along the time dimension, generating a substantial number of useful convolutional features, which are then passed on to subsequent layers in higher quality and denser form. The batch normalization layer helps alleviate internal covariate shifts originating from the convolutional layer. The pooling layer compresses the convolutional features, to some extent, to avoid overfitting. The ReLU activation function mitigates the gradient vanishing problem, making the network easier to train. Finally, the flatten layer transforms all the features into a vector format that meets the input requirements of BiLSTM, which feeds into the subsequent BiLSTM layers.

To understand more easily how they work, their structure is schematically shown in Fig. 1(a).

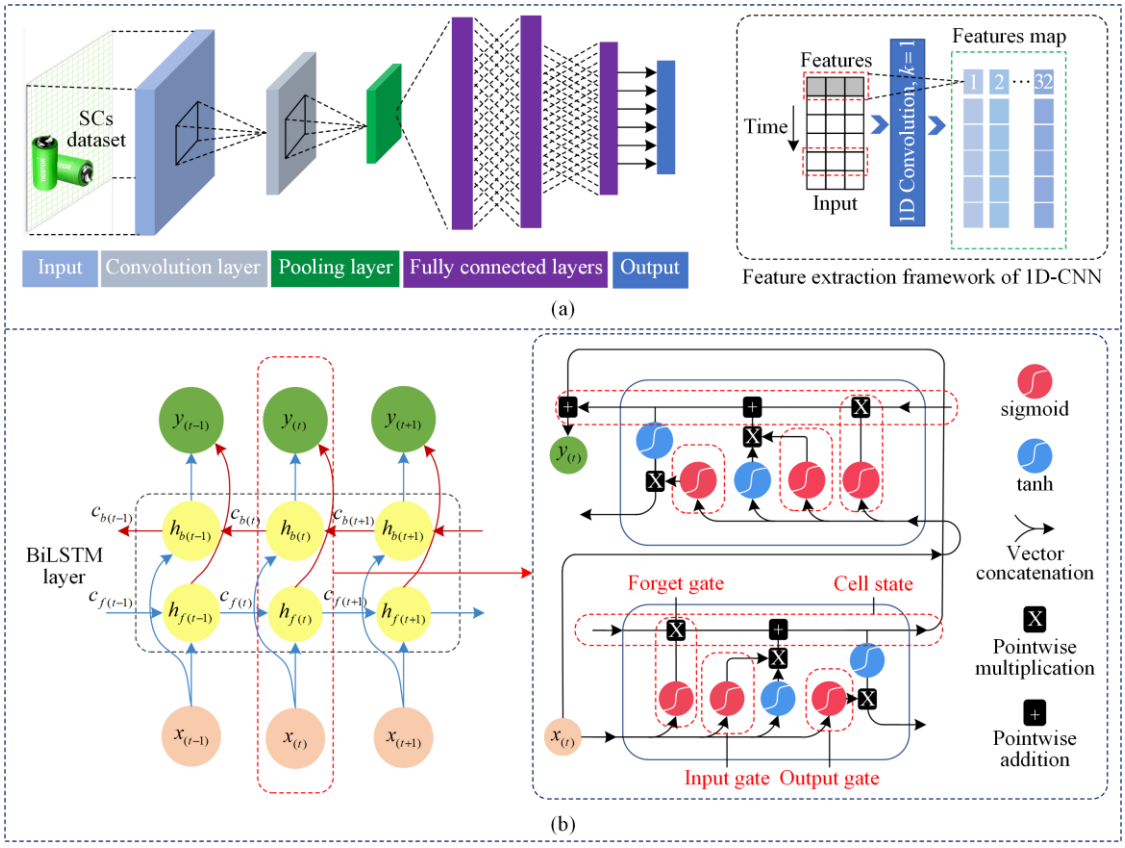

Fig. 1. Schematic diagram of the internal structure of the network. (a) Schematic diagram of the structure of 1D-CNN. (b) Schematic diagram of the structure of BiLSTM.

B. BiLSTM Neural Network

LSTM models are widely used for processing and predicting long time series data because of their memory function and their ability to easily learn long-term dependencies [59]. In the LSTM network, the forgetting gate is responsible for analyzing the information of the memory cell and deciding whether to retain or forget the information; updating the state of the memory cell is handled by the input gate; and the output gate is responsible for controlling the output [60]. To solve the problem that the LSTM model only utilizes the past information of time series data, BiLSTM is proposed, which integrates the forward and backward information based on the whole time series, and is more advantageous for long time series data. 1D-CNN automatically extracts effective features from time series data as input to the BiLSTM network, learns the important parts of the sequence seen so far, and forgets the unimportant parts. Thus, it can discover and synthesize the relationship between input and output sequences. The internal structure of BiLSTM is shown in Fig. 1(b). In the two-layer LSTM, the past sequence information is contained in the hidden layer in the forward time direction and the current sequence information is computed. The future sequence information is sent to the hidden layer in the reverse time direction, and the reverse sequence information is added to the computation. Finally, the output layer outputs the values determined by the two LSTM networks. The BiLSTM network can obtain the final output by integrating the forward output results and the reverse output results. The principle of the reverse process is the same as that of the forward process, but the order is reversed. The symbol of the reverse process can be expressed by subscript *b* instead of *f*. And by adding a recurrent dropout layer, overfitting can be prevented, and the generalization ability of the module is improved. See [61] for more on BiLSTM.

C. Honey Badger Algorithm

The honey badger algorithm is a new intelligent optimization algorithm. Research has shown the effectiveness of HBA in solving complex search space optimization problems. Compared with more than a dozen famous metaheuristic algorithms, HBA has a significant advantage in terms of convergence speed and exploration-exploitation balance. The algorithm mainly conducts optimization by simulating the intelligent foraging behavior of honey badgers and has characteristics such as strong optimization ability and fast convergence speed. The overall candidate solution is shown in (1), and the number of candidate solutions is represented by $\boldsymbol{P}$:

$$\boldsymbol{P}=\begin{bmatrix} x_{11} & \cdots & x_{1D} \\ \vdots & & \vdots \\ x_{n1} & \cdots & x_{nD} \end{bmatrix} \tag{1}$$

where D represents the number of parameters to be optimized and n represents the number of candidate solutions.

The ith position of the honey badger is denoted by x_i. First, in the initialization stage, the parameters to be optimized are initialized according to:

$$x_i = L_{\mathrm{lb}_i} + r_1(U_{\mathrm{ub}_i} - L_{\mathrm{lb}_i}) \tag{2}$$

where r_1 is a random number between 0 and 1; while U_{ub_i} and L_{lb_i} are the upper and lower bounds of the search space, respectively.

Then the intensity I is defined, I_i is the trend from the current value to the target value and is defined by:

$$I_i = r_2 \times \frac{S}{4\pi d_i^2} \tag{3}$$

where r_2 is a random number between 0 and 1; S is source strength; d_i represents the difference between the target parameter and the ith parameter. And there are:

$$\begin{cases} S = (x_i - x_{i+1})^2 \\ d_i = x_{\mathrm{prey}} - x_i \end{cases} \tag{4}$$

where x_{prey} is the global optimal value of the ith parameter.

The factor α, which decreases with the number of iterations, is updated by (5) to reduce the randomization over time and to ensure a smooth transition from exploration to exploitation.

$$\alpha = C^{\frac{t}{t_{\max}}} \tag{5}$$

where α is the density factor controlling the time-varying randomization; $C \geqslant 1$ (default $C = 2$); and $t_{\max}$ is the maximum number of iterations.

To avoid getting trapped in a local optimum region, a flag F that changes the search direction is used, thus enabling more opportunities for the agent to strictly scan the search space.

$$x_{\mathrm{new}} = x_{\mathrm{prey}} + F\beta I x_{\mathrm{prey}} F r_3 \alpha d_i \left|\cos(2\pi r_4)\left[1-\cos(2\pi r_5)\right]\right| \tag{6}$$

where x_{new} is the updated value of x_{prey}, which is the optimal value; $\beta \geqslant 1$ (default $\beta = 6$) represents the performance of the algorithm; r_3, r_4, r_5 are three random numbers between 0 and 1; and there is:

$$F = \begin{cases} 1, & r_6 \leqslant 0.5 \\ -1, & \text{otherwise} \end{cases} \tag{7}$$

where r_6 is a random number between 0 and 1.

The second stage is the honey stage and the mathematical expression is:

$$x_{\mathrm{new}} = x_{\mathrm{prey}} + F r_7 \alpha d_i \tag{8}$$

where r_7 is a random number between 0 and 1.

The detailed optimization process of HBA is shown in Fig. 2.

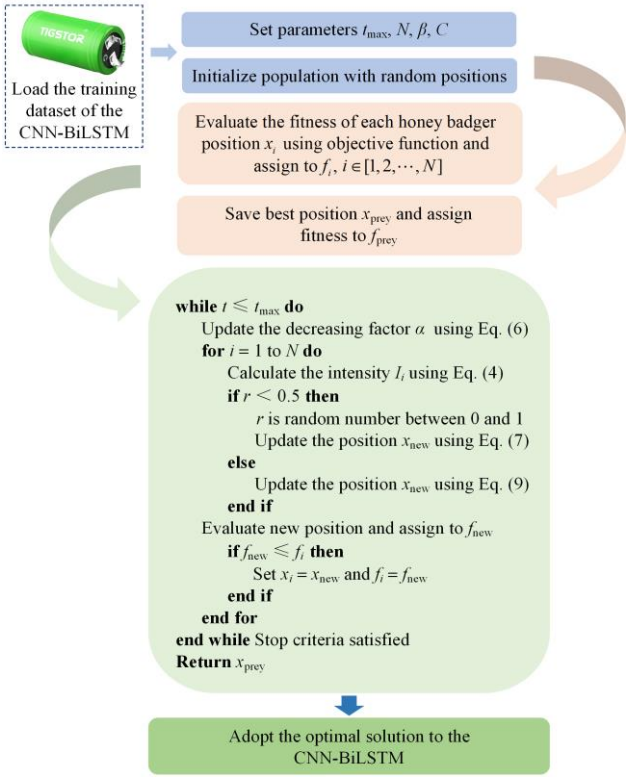

Fig. 2. Schematic diagram of the optimization process using HBA.

The CNN-BiLSTM model has many parameters that need to be adjusted, including learning rate, number of neural network layers, number of convolution layers, convolution kernel size, batch size, and maximum number of training epochs, etc. The improved HBA is used to optimize the hyperparameters of the model. The first stage is the initialization stage, which involves initializing the number N of candidate solutions and the parameters x_i to be optimized. Next, set the maximum number of iterations t_{max}, the parameter β that determines the search capability, and the constant C that affects the smooth transition of the density factor. Since β and C have a significant impact on HBA performance, these two parameters need to be set carefully [62]. As shown in Fig. 3(a), by comparing the fitness of HBA for β and C under different situations, the optimal parameter values are $\beta = 6$ and $C = 2$ respectively. Then the candidate solution is obtained through the objective function and assigned a value, the optimal solution is saved and assigned a corresponding fitness value, the density factor is updated and the search intensity is calculated. Then, determine the size of the parameter r_i value, and use formulas (6) and (8) respectively to update the candidate solutions. Within the maximum number of iterations, the objective function is further used to solve and assign values, and compared with the optimal solution, and updated to obtain the optimal solution for the hyperparameters of the CNN-BiLSTM model. The improved HBA optimization algorithm can automatically search the hyperparameter space more efficiently and systematically explore high-performance hyperparameter combinations. Therefore, the introduction of the improved HBA optimization algorithm further improves training efficiency. The changes in each optimized parameter are shown in Fig. 3(b), At the same time, combined with the final experimental results, it can be seen that the improved HBA optimization algorithm further improves the prediction accuracy and matching degree of the model by optimizing the hyperparameters of the proposed model.

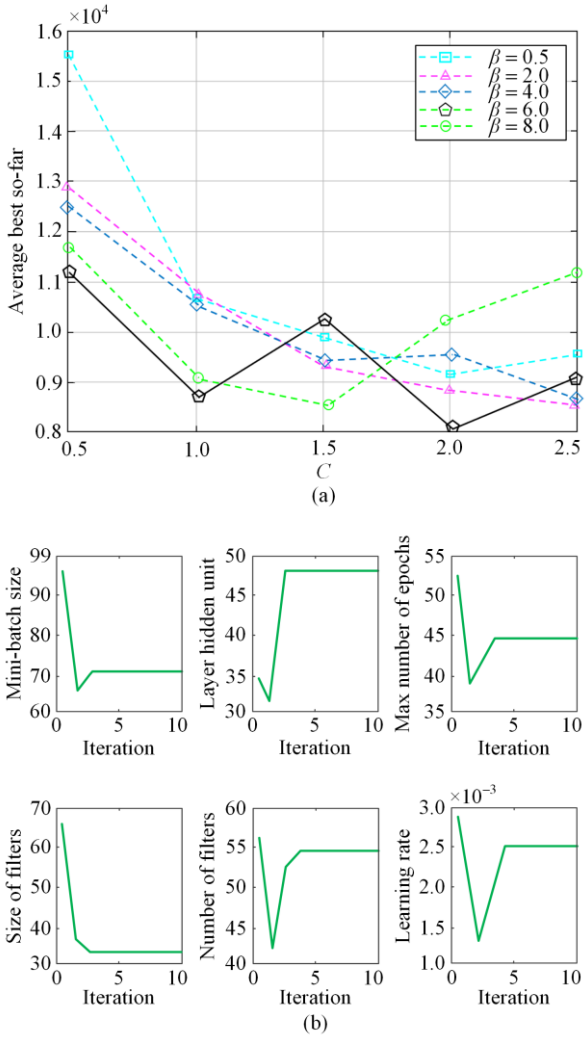

Fig. 3. (a) HBA fitness to parameters β and C. (b) Parameter tuning process under HBA.

D. Opposition Based Learning

OBL is a learning method that utilizes opposition between objects. In metaheuristic algorithms, opposing candidate solutions are obtained in the search space. The main objective of this method is to make the initial random solution more similar to the ideal solution. Randomly generating a solution often leads to inefficient exploration patterns that revisit regions in the search space that are not promising. OBL considers both a candidate solution and its opposite solution at the

same time. Experimental results show that if no prior knowledge is used to optimize the problem, an opposite candidate solution has a higher chance of reaching the global optimum than a random solution. Therefore, introducing a random solution and its corresponding opposite solution is more promising than introducing two independent randomly generated solutions.

Suppose y is a real number in range $[a, b]$, the opposite point of y denoted as $\bar{y}$ is defined as follows:

$$\bar{y} = a + b - y \tag{9}$$

If opposite numbers are defined in n dimensions, the concept of opposite point can be generalized to n-dimensional space, where $n \geqslant 2$. Given an n-dimensional vector $\boldsymbol{\Gamma} = \{y_1, y_2, \cdots, y_n\}$ with $y_i \in [a_i, b_i]$, where $i = 1, 2, \cdots, n$. $\boldsymbol{A} = \{\alpha_1, \alpha_2, \cdots, \alpha_n\}$ and $\boldsymbol{B} = \{b_1, b_2, \cdots, b_n\}$ are two boundary vectors. The opposite vector of $\boldsymbol{\Gamma}$ is defined as $\bar{\boldsymbol{\Gamma}} = \{\bar{y}_1, \bar{y}_2, \cdots, \bar{y}_n\}$, i.e.,

$$\bar{\boldsymbol{\Gamma}} = \boldsymbol{A} + \boldsymbol{B} - \boldsymbol{\Gamma} \tag{10}$$

where $\bar{y}_i = a_i + b_i - y_i$, and y_i is real numbers between a_i and b_i.

HBA combined with OBL is used to converge to the best solution in the search space and allows scanning of the search space from different directions. As shown in Fig. 4, the boundary of the search space for the problem changes according to the fitness values of the random and opposite candidate solutions in OBL. By jumping to different parts of the search space in HBA-OBL, getting stuck in local optima can be avoided. OBL can be adapted to different task requirements by adjusting the loss function, while HBA can accelerate the update process of the loss function. At the same time, OBL can help the model better distinguish between positive and negative samples, and HBA can speed up the training process. Combining these two algorithms can realize a more flexible and effective loss function design, which can enable the model to converge faster to the optimal solution.

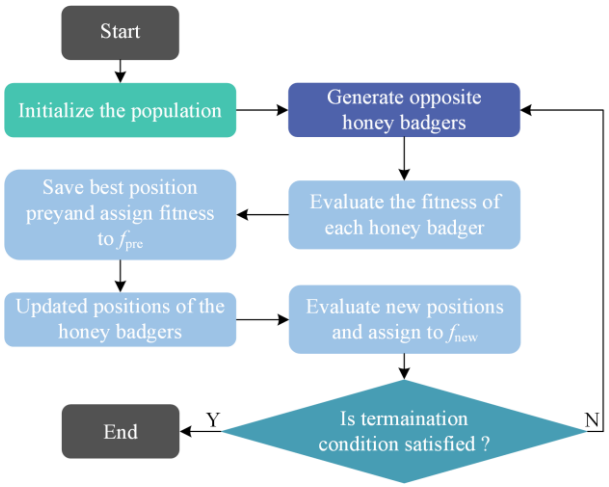

Fig. 4. Schematic diagram of the optimization process using improved HBA.

E. Recurrent Dropout

Dropout is a classical technique for reducing overfitting by randomly setting some input cells of a layer to zero, thereby breaking spurious correlations within the data of that layer. How to use dropout properly in recurrent networks is a key issue. Reference [63] proposes a correct method of using dropout in recurrent neural networks for the first time: a consistent dropout mask (same pattern of dropped units) should be used for each time step. Specifically, the non-time-varying dropout mask should be applied to the internal recurrent activations of the layer (called a recurrent dropout mask). Classic dropout is located between the input and hidden layers, controlling the dropout rate of neurons in the input linear transformation. Recurrent dropout is between hidden layers, controlling the dropout rate of neurons in the linear transformation of the recurrent state. The principle and schematic diagram of its structure is shown in Fig. 5. This allows the network to propagate its learning error correctly over time without corrupting the error signal, thereby preventing overfitting and facilitating the learning process.

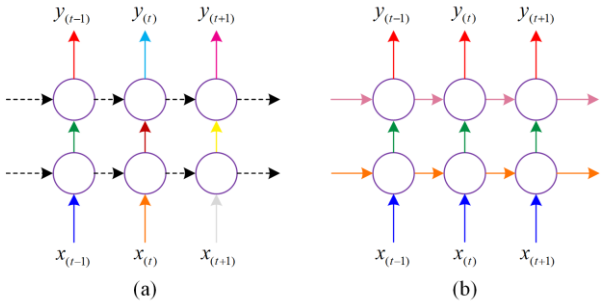

Fig. 5. The schematic diagram above illustrates. (a) the standard dropout. (b) the recurrent dropout structures.

In Fig. 5, each circle represents an LSTM unit, and the horizontal arrows represent time dependencies (cyclic connections). Vertical arrows indicate inputs and outputs. Colored connections represent dropped inputs, and different colors correspond to different dropout masks. The dashed line corresponds to a standard connection with no dropout on the cyclic layer, while the recurrent dropout uses the same dropout mask at each time step, including the cyclic layer.

F. HBA-CNN-BiLSTM Hybrid Neural Network

A well-designed combinatorial neural network can leverage the unique strengths of each component network, allowing them to complement each other. Therefore, we propose an improved CNN-BiLSTM combined network, where the CNN analyzes the time series data in the input model and its output serves as the input of the BiLSTM. The CNN identifies and extracts the desired features during the training phase, and the BiLSTM determines the information that needs to be analyzed and stored. CNN possesses powerful feature extraction capabilities, excelling in collecting local

variables through convolution operations and preserving all local clues as feature maps. BiLSTM comprehensively captures the correlations and long-term dependencies within a sequence by leveraging bidirectional information flow. The improved HBA optimization algorithm can automatically search the hyperparameter space more efficiently and systematically explore high-performance hyperparameter combinations, further improving training efficiency and reducing the overall processing time of the model's time series data. At the same time, the improved HBA is used to optimize the hyperparameters of the network, further enhancing the robustness and scalability of the model. Therefore, the proposed model not only extracts features and enriches local details but also enhances the global perception capability of the model.

In the process of estimating the SOH and predicting the RUL of supercapacitors, the preprocessed raw data of the supercapacitors serves as the input feature variables for the model. The output observation dataset used to construct the model consists of a series of available capacities of the supercapacitors. First, a flexible supercapacitor degradation state space model is established using the proposed algorithm for SOH estimation. Then, the relationship between the cycle count and the feature variables extracted by CNN is reconstructed, and the feature variables are updated and inputted into the proposed model. The degradation features of the supercapacitor are continuously updated, and the failure time point is obtained from the performance degradation curve by setting a degradation threshold. The remaining useful life prediction result is obtained by inferring the time interval between the existing degradation amount and the degradation threshold through the model. Finally, the robustness and reliability of the proposed framework are validated using datasets from different operating conditions and cycle counts. It is important to note that the model needs to be trained in advance to enable online prediction of the health condition of the supercapacitor. The improved HBA-CNN-BiLSTM model is proposed in this paper, which the structure as shown in Fig. 6.

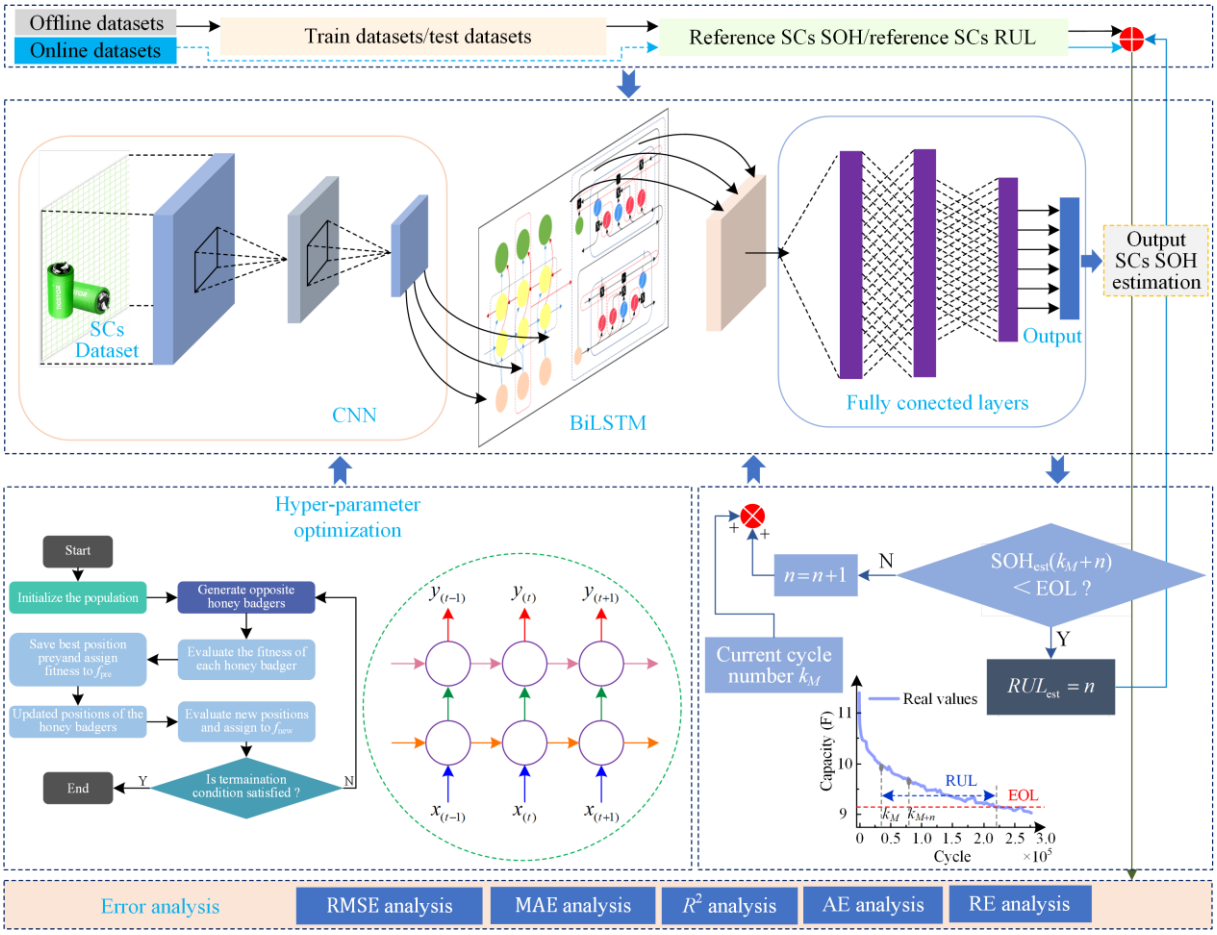

Fig. 6. The flowchart of improved HBA-CNN-BiLSTM for SOH estimation and RUL prediction.

III. Supercapacitor Aging Test and Analysis

A. Hardware System for Aging Test Experiments

The supercapacitor aging state testing system consists of three main components: the testing system, the upper computer, and the high and low temperature chamber. Due to the influence of temperature, voltage, and frequency on supercapacitors, the supercapacitor capaci-

tors are chosen to be measured under the same environment respectively to ensure the consistency of parameter measurement standards.

The testing system utilized is the REPOWER HRCDS-5 V, which is capable of discharging supercapacitors using constant current (CC), constant voltage (CV), and constant power (CP) modes. This system boasts a variety of built-in test modes, including CC-CV, CC, and CP charging-discharging tests, capacitance measurements, and direct current resistance tests specifically designed for supercapacitors. Each testing mode undergoes step transitions based on the set time, voltage, current, or power conditions. The data collection includes feedback on testing steps, status, voltage, current, capacitance, and other data. There are also various flexible sampling options available, which can be determined based on time, voltage, current, or capacitance conditions. The CPU model of the upper computer is Intel i7-11700, which is used to store and process the data; the high and low-temperature chamber is used to provide a specific temperature environment for the aging state test of the supercapacitor. The TIGSTOR supercapacitor, model TIG-1W160P010R01, was selected for this experiment. The capacity of the supercapacitor is 10 F, the rated voltage is 2.7 V, and the operating temperature range is [–40°C, 70°C]. Charge the supercapacitor in a constant current mode of 3 A until the voltage reaches 2.7 V, then continue charging in a constant voltage mode. Perform multiple charge and discharge tests at different temperatures and voltages, maintaining a discharge depth of 50%. Conduct these tests in the same environment without taking vibration into consideration, repeating the cycles hundreds of thousands of times. We arranged and combined four different voltage and temperature conditions, and selected four supercapacitors under each condition to observe their aging trends. Consequently, we collected aging experimental data for a total of 64 supercapacitors. Table I presents one set of cyclic test conditions for the supercapacitors under the four different voltage and temperature conditions. The test platform is shown in Fig. 7(a).

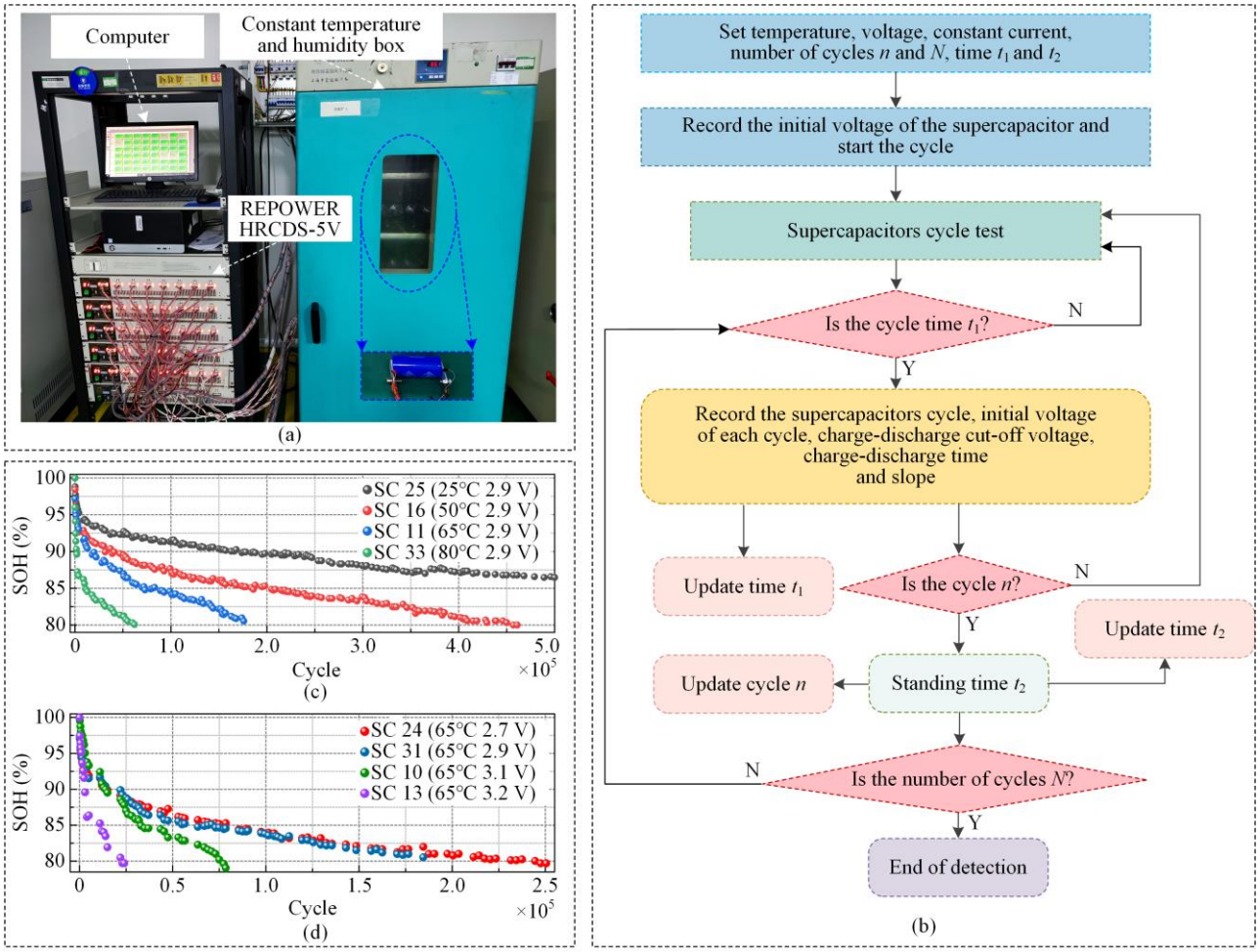

Fig. 7. Supercapacitor aging test experiment. (a) Supercapacitor aging test system (supercapacitor charging/discharging with CC-CV charging protocol at different temperatures and voltages). (b) Schematic diagram of the experimental procedure. (c) Capacity degradation trajectory of supercapacitor with an increasing number of cycles at 25°C, 50°C, 65°C, and 80°C. (d) Capacity degradation trajectory of supercapacitor at 2.7 V, 2.9 V, 3.1 V, and 3.2 V capacitors with increasing cycle times.

TABLE I
CYCLIC TEST CONDITIONS OF SUPER CAPACITORS

Supercapacitor number	Voltage (V)	Temperature (℃)
SC 1	3.2	25
SC 2	3.2	50
SC 3	2.9	80
SC 4	2.7	25
SC 5	3.2	80
SC 6	2.7	80
SC 7	2.7	50
SC 8	3.1	25
SC 9	3.1	50
SC 10	3.1	65
SC 11	2.9	65
SC 12	3.1	80
SC 13	3.2	65
SC 14	2.7	65
SC 15	2.9	25
SC 16	2.9	50

B. Aging Characteristics Analysis

In this experiment, the supercapacitor was cyclically charged and discharged under different temperature and voltage conditions using the CC-CV charging protocol, and the experimental process is shown in Fig. 7(b). The aging trends of the capacitors under different temperature and voltage conditions were analyzed, and the results are shown in Fig. 7(c) and Fig. 7(d). The results reveal that the aging rate of the supercapacitor is closely related to temperature and voltage, and the aging accelerates as the temperature increases. This is because the movement of ions in the electrolyte and various reactions occurring on the electrode surface are affected by the temperature. Meanwhile, supercapacitors cannot operate at overvoltage for a long time.

The degradation trend of capacity is similar at different voltages and temperatures, i.e., the SOH of the supercapacitor follows a similar change pattern. Therefore, the method proposed in this paper applies to SOH estimation and RUL prediction of supercapacitors under different operating environments.

IV. EXPERIMENTAL RESULTS AND ANALYSIS

In this section, we present the results of SOH estimation and RUL prediction of supercapacitors using LSTM, BiLSTM, CNN-BiLSTM, and HBA-CNN-BiLSTM models. The initial parameters of the CNN network are filters of 32, kernel_size of 3, strides of 1, activation is 'ReLU', the pool_size in MaxPooling1D is 3, the number of hidden layer cells in BiLSTM is 32, dropout is 0.1, recurrent_dropout is 0.5, the initial value of learning rate is 0.01. The training time is calculated by the time. time function in Python Time Library. The offline data of the supercapacitor is divided into training and test sets, which are 70% and 30%, respectively. To demonstrate the generalization capability of this model, two datasets, SC 14 and SC 15, at different temperatures and voltages, were randomly selected for validation and error analysis, and the metrics root mean square error (RMSE), mean absolute error (MAE), R^2, absolute error (AE), and relative error (RE) were used to measure the performance of the model.

A. *Evaluation Metrics*

e_{RMSE} (the value of RMSE) is used to represent the statistical value that causes the deviation from the mean to be too large or too small. The magnitude of e_{RMSE} represents the average difference between the predicted and true values, and the smaller the value, the more accurate the model and the more stable the model. The calculation formula is as follows:

$$e_{\mathrm{RMSE}} = \sqrt{\frac{1}{N}\sum_{n=1}^{N}(y_n - \hat{y}_n)^2} \tag{11}$$

e_{MAE} (the value of MAE) can suppress the problem of errors canceling each other out by taking the average of the absolute errors between the predicted and true values. It provides a clear reflection of the actual situation of the predicted value errors: the smaller its value, the higher the model's accuracy. The calculation formula is as follows:

$$e_{\mathrm{MAE}} = \frac{1}{N}\sum_{n=1}^{N}\left|y_n - \hat{y}_n\right| \tag{12}$$

The R^2 coefficient of determination is a visual representation of the correlation between the model and the true value. The higher the value of the R^2 coefficient of determination, the more accurate the model is. If $R^2 = 1$, it means that the model predicts the true value exactly correctly and all observations fall on the regression line. $R^2 = 0$ means that the model predicts the true value with poor accuracy. $R^2 < 0$ means that there is a lack of linear correlation between the data. It is widely used in model prediction evaluation because it has no magnitude problem and compensates for the defect that prediction cannot be made due to the presence of several 0 values in the data. The calculation formula is as follows:

$$R^2 = 1 - \frac{\sum_{n=1}^{N}(y_n - \hat{y}_n)^2}{\sum_{n=1}^{N}(y_n - \bar{y}_n)^2} \tag{13}$$

where y_n represents the true value; $\hat{y}_n$ represents the predicted value; and $\bar{y}_n$ represents the arithmetic mean of the dependent variable in the original data set. In this paper, e_{RMSE}, e_{MAE} and R^2 are used as performance metrics for estimation and prediction accuracy.

The accuracy of the supercapacitor RUL prediction at a specific capacity threshold can be represented by the difference between the actual and predicted number of cycles. Therefore, we introduce e_{AE} and e_{RE} (the values of AE and RE) for evaluation.

$$e_{\mathrm{AE}} = \left|e_{\mathrm{RUL_{re}}} - e_{\mathrm{RUL_{pr}}}\right| \tag{14}$$

$$e_{\mathrm{RE}} = \frac{\left| e_{\mathrm{RUL_{re}}} - e_{\mathrm{RUL_{pr}}} \right|}{e_{\mathrm{RUL_{re}}}} \times 100\% \tag{15}$$

where $e_{\mathrm{RUL_{re}}}$ denotes the actual value and $e_{\mathrm{RUL_{re}}}$ denotes the predicted value.

B. The Estimation Results and Analysis of SOH

In this study, experimental data from supercapacitors under different operating conditions were randomly used to train the LSTM, BiLSTM, CNN BiLSTM, and HBA-CNN-BiLSTM models to predict the capacity and further determine the SOH values of the supercapacitors. The first 70% of the supercapacitor dataset was allocated for offline training of the models, while the remaining dataset was used for online testing. To comprehensively evaluate the robustness and effectiveness of the models, all methods employed the same offline training strategy, thus enabling a comprehensive assessment of the models' robustness and effectiveness. e_{RMSE} and e_{MAE} are the evaluation indexes of accuracy, and the R^2 decision coefficient is used to reflect the correlation between the model and the real values. The experimental results are shown in Fig. 8, and the specific error values are presented in Table II.

TABLE II
SC 4 (2.7 V, 3 A, 25°C) SUPERCAPACITOR STATE OF HEALTH AND REMAINING USEFUL LIFE PREDICTION RESULTS

Method	e_{RMSE}	e_{MAE}	R^2	e_{RULre} ($\times 10^5$)	e_{RULpr} ($\times 10^5$)	e_{AE} ($\times 10^3$)	e_{RE} (%)
LSTM	0.0297	0.0255	0.9761	2.227	2.16	6.7	3.009
BiLSTM	0.0261	0.0235	0.9864	2.227	2.17	5.7	2.5594
CNN-BiLSTM	0.0238	0.0207	0.9894	2.227	2.19	3.7	1.6614
HBA-CNN-BiLSTM	0.0149	0.0121	0.9943	2.227	2.22	0.7	0.3143

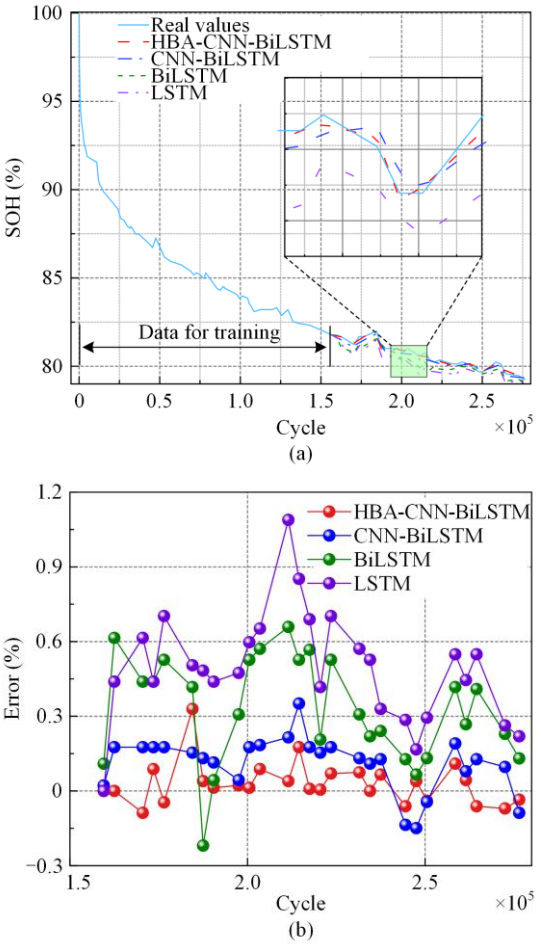

Fig. 8. Comparison of SOH estimation results for SC 4 supercapacitor (2.7 V, 3 A, 25°C) for four different methods. (a) SOH estimation result. (b) SOH estimation error.

As can be seen from Fig. 8, the LSTM, BiLSTM, CNN-BiLSTM, and HBA-CNN-BiLSTM models all have good fits for the capacity decay curve of supercapacitors.

In comparison, the proposed HBA-CNN-BiLSTM model can better fit the overall trend of the supercapacitor aging curve. This is because the hybrid neural network can fully utilize the unique advantages of each network, and thus has higher prediction stability and accuracy. The hybrid neural network optimized by the improved HBA algorithm has the highest estimation accuracy, with e_{RMSE} of 0.0149, e_{MAE} of 0.0121, and R^2 of 0.9943. Compared with the network not optimized by the improved HBA algorithm, e_{RMSE}, and e_{MAE} are reduced by 0.0089 and 0.0086, respectively. At the same time, the improved R^2 value further proves the superiority of the model. To verify the generalization ability of the model, we randomly selected an untrained supercapacitor dataset under two different temperature and voltage operating conditions. The experimental results are shown in Figs. 9(a) and (b), and the specific error values are presented in Tables III and IV. To further evaluate the models, Figs. 9(c) and (d) respectively display the boxplots of the prediction errors and the distribution of the errors. Taking all factors into account, the proposed models exhibit smaller prediction errors and better prediction performance.

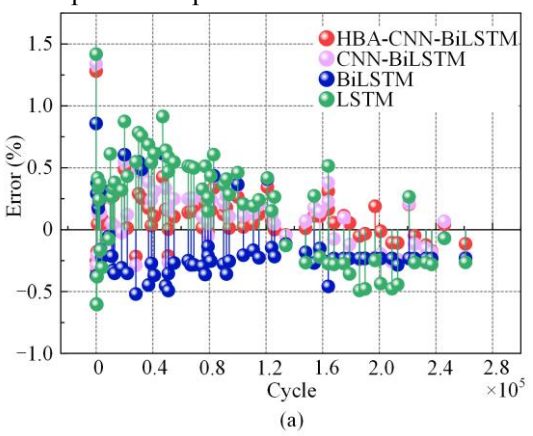

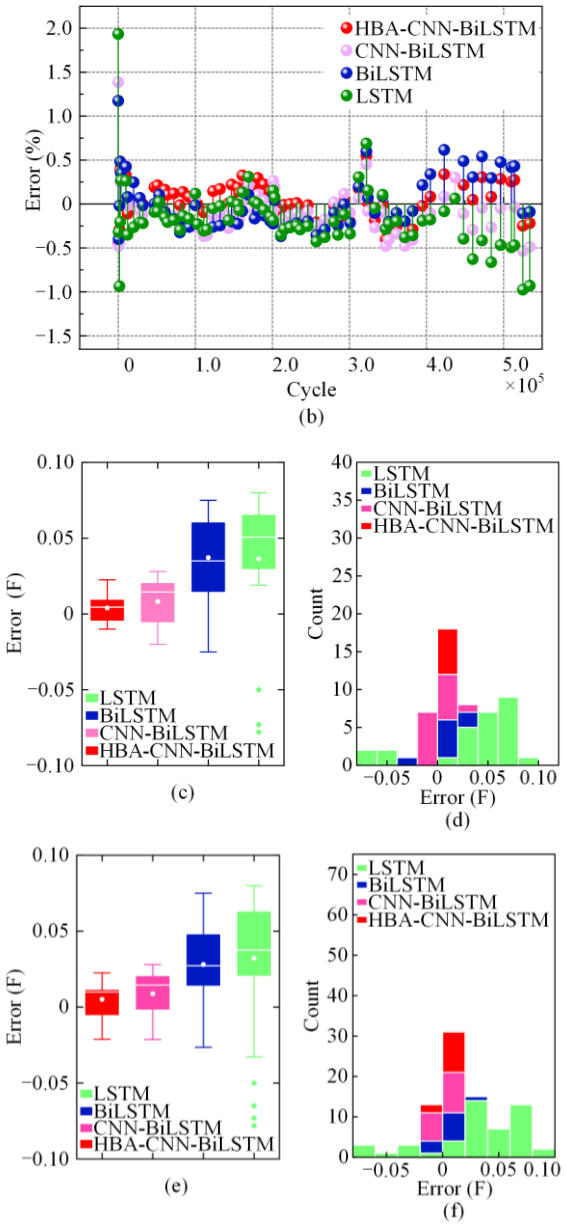

Fig. 9. SOH estimation results and errors of supercapacitor under different methods. (a) SC 14 (2.7 V, 3A, 65℃). (b) SC 15 (2.9 V, 3 A, 25℃). (c) Boxplot analysis of the prediction errors for the four models under SC 14 experimental data. (d) Analysis of the distribution of prediction errors for the four models under SC 14 experimental data. (e) Boxplot analysis of the prediction errors for the four models under SC 15 experimental data. (f) Analysis of the distribution of prediction errors for the four models under SC 15 experimental data.

Although each model has different performances for supercapacitors under different working conditions, our proposed HBA-CNN-BiLSTM hybrid neural network model consistently achieves better accuracy.

In addition, the training time can reflect the training and prediction efficiency of the model. The training time of the proposed model is 20.5% lower than that of the BiLSTM model. BiLSTM processes time series data sequentially, while CNN, due to its intrinsic convolutional nature, can perform parallel computations. This parallel computation enables faster processing of time series data, thereby expediting the training process. The initial feature extraction accomplished by CNN reduces the input dimensionality for subsequent BiLSTM layers, resulting in higher computational efficiency. Furthermore, the subsequent BiLSTM layers can focus on capturing long-range dependencies and higher-level temporal representations, enabling BiLSTM to handle more concise and information-rich input data, thus enhancing training efficiency. The introduction of the improved HBA optimization algorithm eliminates the manual trial-and-error process of adjusting hyperparameters, allowing for a more efficient automatic search of the hyperparameter space and systematic exploration of high-performance hyperparameter combinations. Therefore, the introduction of the improved HBA optimization algorithm further improves training efficiency and reduces the overall processing time of time series data by the neural network model. This is of great significance for the health detection of supercapacitors and better promotion of applications. The SOH estimation results show that the HBA-CNN-BiLSTM model is effective and robust, providing a solid foundation for predicting the supercapacitor RUL.

C. The Prediction Results and Analysis of RUL

Accurately predicting the RUL of supercapacitors is crucial for predictive maintenance. It determines the number of remaining available charge/discharge cycles before performance degrades to an unacceptable level, and guides proactive replacement to avoid failures. This prediction also helps to maximize the lifespan of supercapacitors by indicating when to take appropriate measures. When the capacity value or SOH reaches the failure threshold, the estimated number of charge/discharge cycles marks the end of RUL prediction for that supercapacitor. The RUL prediction results are shown in Fig. 10, and the specific error values are presented in Table II.

To validate the generalization capability of the model for RUL prediction, two randomly selected untrained supercapacitors were tested under different temperature and voltage conditions. The experimental results are shown in Fig. 11, and the specific error values are presented in Table III and Table IV. By comparing the RE values in the tables, it can be observed that the proposed model also demonstrates high robustness in the RUL prediction of supercapacitors, with RE values of 0.3193 and 0.3271 respectively, which are excellent for supercapacitors with tens of thousands of cycles or more. This robustness is attributed to the model's high reliability in estimating SOH. Therefore, we can infer that accurate capacity prediction holds significant im-

portance and precise SOH estimation serves as a crucial foundation for accurate RUL prediction.

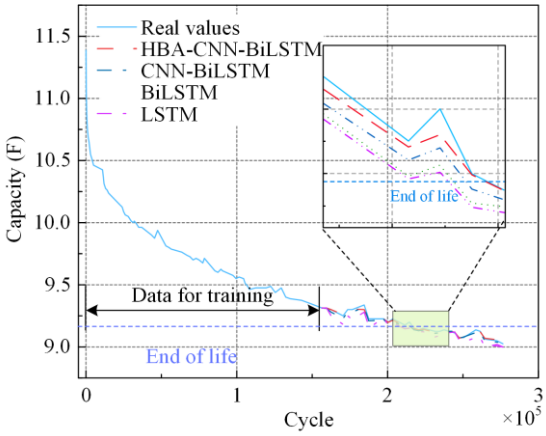

Fig. 10. Predicted supercapacitor degradation data for SC4 (2.7 V, 3 A, 25°C) under different methods.

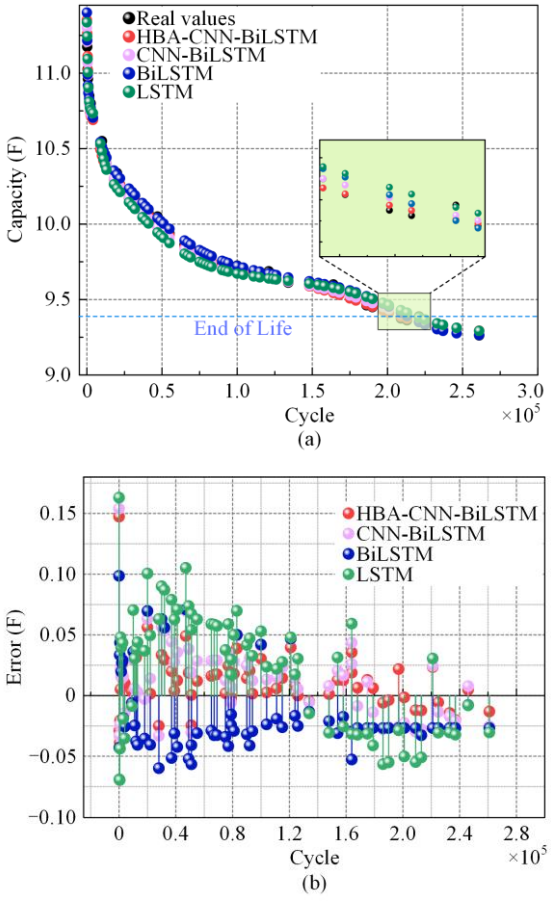

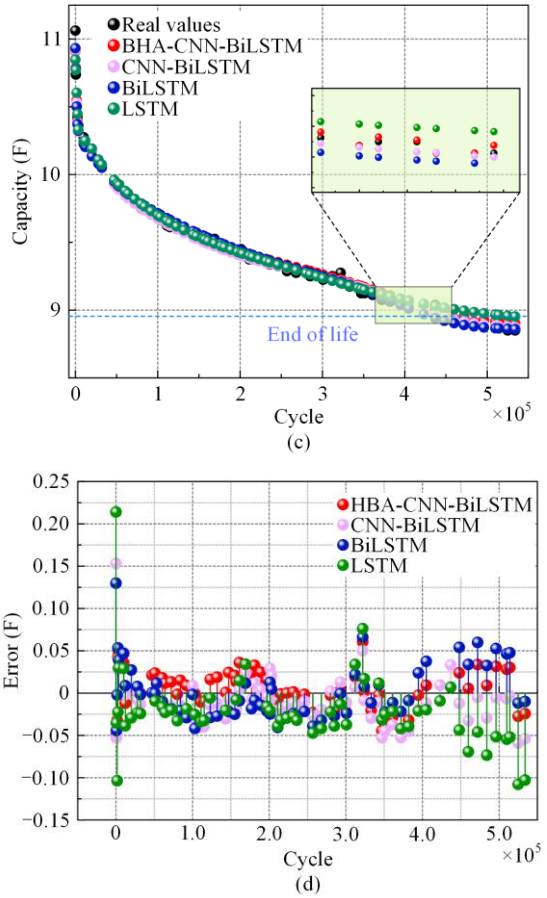

Fig. 11. Predicted results and errors of supercapacitor degradation data for SC 14 (2.7 V, 3 A, 65°C) and SC 15 (2.9 V, 3 A, 25°C) under different methods. (a) and (b) SC14 (2.7 V, 3 A, 65°C). (c) and (d) SC 15 (2.9 V, 3A, 25°C).

The above experimental results indicate that the proposed method is applicable to supercapacitors under different operating conditions, and the HBA-CNN-BiLSTM shows high robustness in both SOH estimation and RUL prediction. Since the supercapacitor data under this condition are not trained, the initial prediction error is relatively large. Moreover, LSTM has certain limitations when dealing with long-term sequence problems and unresolved gradient issues. Therefore, there are still certain deficiencies in the prediction of large-scale data such as supercapacitors. For SC 15 with large data samples, the proposed model demonstrates significant advantages over LSTM and BiLSTM. When the failure threshold is reached, the RE between the prediction and the true value is only 0.3271%, outperforming the other three methods.

TABLE III
SC 14 (2.7 V, 3 A, 65°C) SUPERCAPACITOR STATE OF HEALTH AND REMAINING USEFUL LIFE PREDICTION RESULTS

Method	e_{RMSE}	e_{MAE}	R^2	e_{RULre} ($\times 10^5$)	e_{RULpr} ($\times 10^5$)	e_{AE} ($\times 10^3$)	e_{RE} (%)
LSTM	0.0292	0.0245	0.9781	2.543	2.6251	8.21	3.2284
BiLSTM	0.0271	0.0239	0.9874	2.543	2.48537	5.763	2.2662
CNN-BiLSTM	0.0235	0.0207	0.9894	2.543	2.58121	3.821	1.5026
HBA-CNN-BiLSTM	0.0163	0.0132	0.9986	2.543	2.53488	0.812	0.3193

TABLE IV
SC 15 (2.9 V, 3 A, 25°C) SUPERCAPACITOR STATE OF HEALTH AND REMAINING USEFUL LIFE PREDICTION RESULTS

Method	e_{RMSE}	e_{MAE}	R^2	e_{RULre} ($\times 10^5$)	e_{RULpr} ($\times 10^5$)	e_{AE} ($\times 10^3$)	e_{RE} (%)
LSTM	0.0296	0.0251	0.9783	4.83	5.213	38.3	7.9296
BiLSTM	0.0261	0.0225	0.9878	4.83	4.512	38.1	6.5838
CNN-BiLSTM	0.0228	0.0201	0.9934	4.83	4.757	7.3	1.511
HBA-CNN-BiLSTM	0.0168	0.0131	0.9983	4.83	4.8142	1.58	0.3271

Table V provides a comparative analysis between the proposed method and other recently published methods. The comparison of RMSE values highlights the superiority of the proposed method over the others. The proposed model exhibits higher prediction accuracy under different operating conditions. This is because, in the hybrid model, CNN effectively reduces data scale and filters inputs to extract significant features, thereby comprehensively capturing local and relevant information. As a result, it achieves high prediction accuracy even on untrained datasets. The model further benefits from improved HBA optimization for its hyperparameters, which enhances optimization capabilities and ensures fast convergence.

TABLE V
COMPARISON OF RECENT PUBLICATIONS WITH OUR PROPOSED METHOD

Methods	Refs.	Metric	Error
HHO-LSTM	[3]	RMSE	0.0301
TCN	[4]	RMSE	0.0270
Mixers-BTCN	[13]	RMSE	0.0248
SSA-Elman	[19]	RMSE	0.0295
LSTM-DA	[45]	RMSE	0.0222
BMA-LSTMN	[49]	RMSE	0.0324
BiLSTM	[50]	RMSE	0.0297
HBA-CNN-BiLSTM	Proposed in this paper	RMSE	0.0163

Randomly selecting untrained supercapacitors SC 42, we tested the RUL prediction performance of various models under different starting points. The results of RUL prediction based on four different models from various starting points are shown in Fig. 12. It can be observed that the proposed method demonstrates satisfactory robustness for RUL prediction on a dataset with random starting points. As the starting point values increase, the accuracy of predictions from all models improves. This is because the degradation trend of supercapacitors is more pronounced in the initial stage compared to the later stages. Therefore, as the random starting point value increases, the accuracy of predictions also increases accordingly.

With the continuous development of electronic technology, in the future electrical and electronic architecture, the data processing and algorithm computation functions of the supercapacitor management system (SMS) will be transferred to domain processors, which have more powerful computational capabilities. This will provide opportunities for the practical application of neural networks. Therefore, a comprehensive performance analysis of the above methods is conducted, and evaluation metrics include FLOPs, parameters, training time, and storage size. FLOPs are used to measure computational complexity, and parameters indirectly affect the model's storage size. The storage size is calculated using the os.path.getsize function. Training time represents the training efficiency of the model and is measured using the time.time function. Table VI presents the aforementioned parameters for each model. The proposed model has lower time complexity. CNN can reduce data dimensions while extracting effective features, thereby reducing memory consumption and possessing higher robustness and generalization ability. Compared to other models, the proposed model does not have an advantage in terms of storage size. However, in practical applications, model accuracy and robustness should also be considered. With the continuous development and progress of processors, a reasonable balance needs to be struck based on specific practical application scenarios.

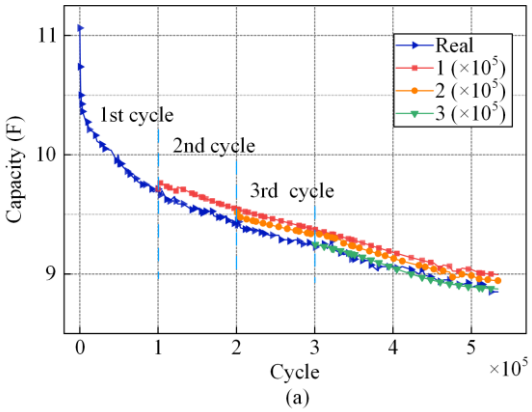

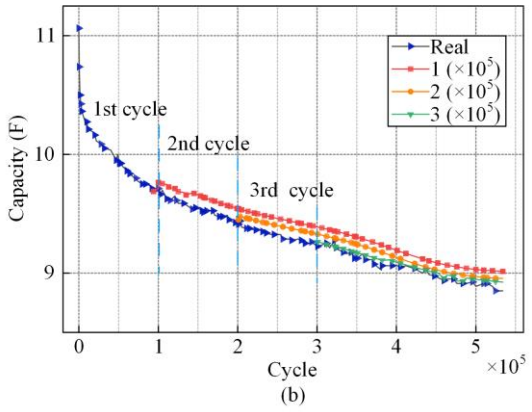

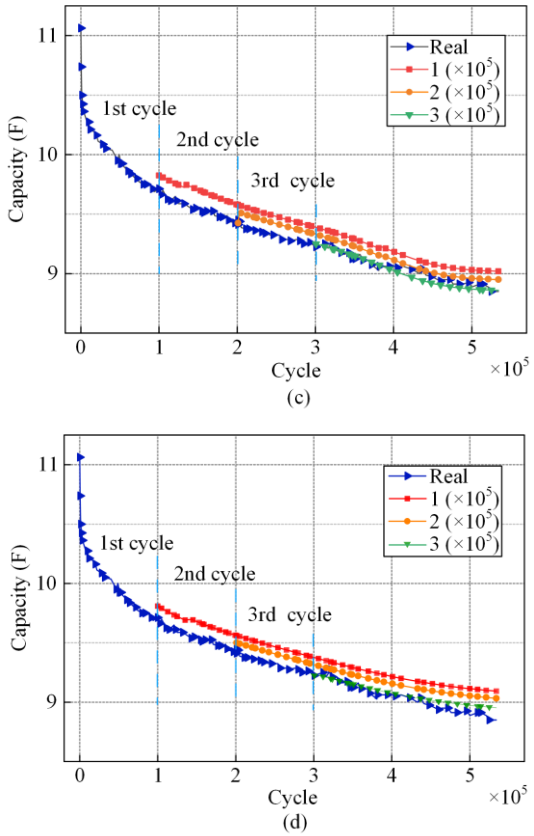

Fig. 12. The RUL prediction results of each model under random starting points for SC 42 (2.9 V, 3 A, 25°C). (a) HBA-CNN-BiLSTM. (b) CNN-BiLSTM. (c) BiLSTM. (d) LSTM.

TABLE VI
COMPREHENSIVE EVALUATION OF THE PROPOSED METHOD

Methods	Performance index			
	FLOPs ($\times 10^6$)	Parameters ($\times 10^6$)	Training time (s)	Storage size (kB)
HBA-CNN-BiLSTM	1.231	0.0258	252	2412
CNN-BiLSTM	1.203	0.0241	316	2136
BiLSTM	0.681	0.0075	354	976
LSTM	0.604	0.0045	301	762

V. CONCLUSION

This research presents a novel HBA-CNN-BiLSTM method that utilizes an improved HBA optimization to estimate and predict the SOH and RUL of supercapacitors. The method combines the architectures of hybrid CNN and BiLSTM networks to address the limitations of capturing only local features and unidirectional temporal features in CNN and LSTM models, respectively. The improved HBA optimizes the hyperparameters of the hybrid network, enhancing model convergence speed and reliability. Recurrent dropout is introduced to prevent overfitting and enable the network to propagate its learning errors over time without disrupting the error signals, thereby promoting the learning process. Different datasets of supercapacitors under various operating conditions were used to test the performance of various models, while untrained data of supercapacitors at different cycle starting points were utilized to verify the generalization ability of the models. The results demonstrate that the proposed model outperforms the other three models in terms of lower error, higher robustness, as well as better training and prediction efficiency. Therefore, it has the potential for further research and development. While the proposed model has advantages in prediction accuracy and efficiency, it exhibits higher complexity and storage size than LSTM, resulting in a greater computational burden. However, with the continuous development of electronic technology, future domain processors will have more powerful computational capabilities, facilitating the practical application of neural networks. Compared to the other three popular algorithms, this hybrid approach has better performance in handling non-smooth and nonlinear time series. The impact of adding convolutional layers is significant for large databases, and the data processing time of the hybrid model is much shorter than that of the BiLSTM network. The experimental results provide sufficient evidence for the effectiveness of the proposed method compared to others.

In future work, it is worth further investigating how to reduce the computational burden, improve model convergence speed, and decrease training time while enhancing prediction accuracy and efficiency. Additionally, compared to lithium-ion batteries, there is a scarcity of publicly available datasets for supercapacitors, and further research is needed to fill this gap. The model proposed in this study has advantages in handling time series problems and can potentially be applied to other similar fields.

ACKNOWLEDGMENT

Not applicable.

AUTHORS' CONTRIBUTIONS

Zhenxiao Yi and Shi Wang: writing original draft, methodology, conceptualization, software, investigation, formal analysis, writing review, and editing. Zhaoting Li: writing review and editing, conceptualization, methodology, supervision, project administration, and funding acquisition. Licheng Wang: writing review and editing. Kai Wang: writing review and editing, conceptualization, methodology, supervision, project administration and funding acquisition. All authors read and approved the final manuscript.

FUNDING

This work is supported by the Zhejiang Province Natural Science Foundation (No. LY22E070007) and the National Natural Science Foundation of China (No.

52007170). And this work was supported by Youth Innovation Technology Project of Higher School in Shandong Province (No. 2022KJ139).

Availability of Data and Materials

Please contact the corresponding author for data material request.

Declarations

Competing interests: The authors declare that the authors have no known competing financial interests or personal relationships that could have appeared to influence the work reported in this article.

Authors' Information

Zhenxiao Yi is currently studying at the School of Electrical Engineering, Qingdao University, Shandong province, China. His research interests include state assessment and remaining useful life prediction of new energy storage devices, distributed microgrid and energy storage.

Shi Wang works at the Institute of Computing Technology, Chinese Academy of Sciences, Beijing, China. His research interests includes knowledge graph, and neural-symbolic dual-process computing.

Zhaoting Li is currently studying computer engineering at the School of Engineering, Brown University, Providence, RI, USA. His research interests include modeling, design, and application of DC-DC converters, LED lighting systems, and energy storage devices.

Licheng Wang works at the College of Information Engineering, Zhejiang University of Technology, Hangzhou, China. His research interests include power system operation and control, renewable energy integration into distribution systems, distributed algorithms, deep reinforcement learning and its application in networked systems.

Kai Wang works at the School of Electrical Engineering, Qingdao University, Shandong province, China. His research interests include state assessment and life prediction of new energy storage devices, energy storage element, storage and conversion of new energy.

References

[1] N. Ma, D. Yang, and S. Riaz *et al*., "Aging mechanism and models of supercapacitors: a review," *Technologies*, vol. 11, no. 2, pp. 38, Mar. 2023.

[2] M. Zhang, Y. Liu, and D. Li *et al*., "Electrochemical impedance spectroscopy: a new chapter in the fast and accurate estimation of the state of health for lithium-ion batteries," *Energies*, vol. 16, no. 4, Feb. 2023.

[3] N. Ma, H. Yin, and K. Wang, "Prediction of the remaining useful life of supercapacitors at different temperatures based on improved long short-term memory," *Energies*, vol. 16, no. 14, Jul. 2023.

[4] C. Liu, D. Li, and L. Wang *et al*., "Strong robustness and high accuracy in predicting remaining useful life of supercapacitors," *APL Materials*, vol. 10, no. 6, pp. 061106-061112, Jun. 2022.

[5] D. Jin, Z. Gu, and Z. Zhang, "Lithium battery health degree and residual life prediction algorithm" *Power System Protection and Control*, vol. 51, no. 1, pp. 122-130, Jan. 2023. (in Chinese)

[6] X. Xie, Y. Ding, and Y. Sun *et al*., "A novel time-series probabilistic forecasting method for multi-energy loads," *Energy*, vol. 306, Oct. 2024.

[7] Y. Liu, L. Wang, and D. Li *et al*., "State-of-health estimation of lithium-ion batteries based on electrochemical impedance spectroscopy: a review," *Protection and Control of Modern Power Systems*, vol. 8, no. 3, pp. 1-17, Jul. 2023.

[8] L. Wang, L. Xie, and Y. Yang *et al*., "Distributed online voltage control with fast PV power fluctuations and imperfect communication," *IEEE Transactions on Smart Grid*, vol. 14, no. 5, pp. 3681-3695, Jan. 2023.

[9] P. Ma, S. Cui, and M. Chen *et al*., "Review of family-level short-term load forecasting and its application in household energy management system," *Energies*, vol. 16, no. 15, Aug. 2023.

[10] C. Liu, Q. Li, and K. Wang, "State-of-charge estimation and remaining useful life prediction of supercapacitors," *Renewable & Sustainable Energy Reviews*, vol. 150, Oct. 2021.

[11] X. Yu, N. Ma, and L. Zheng *et al*., "Developments and applications of artificial intelligence in music education," *Technologies*, vol. 11, no. 2, Mar. 2023.

[12] Z. Yi, Z. Chen, and K. Yin *et al*., "Sensing as the key to the safety and sustainability of new energy storage devices," *Protection and Control of Modern Power Systems*, vol. 8, no. 2, pp. 1-22, Apr. 2023.

[13] J. Gao, D. Yang, and S. Wang *et al*., "State of health estimation of lithium-ion batteries based on mixers-bidirectional temporal convolutional neural network," *Journal of Energy Storage*, vol. 73, Dec. 2023.

[14] Y. Pan, Y. Zhu, and Y. Li *et al.*, "Homonuclear transition-metal dimers embedded monolayer C2N as promising anchoring and electrocatalytic materials for lithium-sulfur battery: first-principles calculations," *Applied Surface Science*, vol. 610, Feb. 2023.

[15] D. Yang, L. Zhang, and L. Wang *et al*., "Recent advances in flexible nanogenerators for microphone and loudspeaker applications," *ACS Applied Electronic Materials*, vol. 5, no. 11, pp. 6063-6078, Oct. 2023.

[16] D. Yang, Y. Shang, and Z. Li *et al*., "Triboelectric nanogenerator assisted by machine learning," *ACS Applied Electronic Materials*, vol. 5, no. 12, pp. 6549-6570, Nov. 2023.

[17] J. Chen, G. Qi, and K. Wang, "Synergizing machine learning and the aviation sector in lithium-ion battery applications: a review," *Energies*, vol. 16, no. 17, Sept. 2023.

[18] J. He, S. Meng, and X. Li *et al*., "Partial charging-based health feature extraction and state of health estimation of

lithium-ion batteries," *IEEE Journal of Emerging and Selected Topics in Power Electronics*, vol. 11, no. 1, pp. 166-174, Feb. 2023.

[19] Y. Guo, D. Yang, and Y. Zhang *et al*., "Online estimation of SOH for lithium-ion battery based on SSA-Elman neural network," *Protection and Control of Modern Power Systems*, vol. 7, no. 3, pp. 1-17, Jul. 2022.

[20] H. Sun, D. Yang, and L. Wang *et al*., "A method for estimating the aging state of lithium-ion batteries based on a multi-linear integrated model," *International Journal of Energy Research*, vol. 46, no. 15, pp. 24091-24104, Dec. 2022.

[21] Y. Liu, J. Sun, and Y. Shang *et al*., "A novel remaining useful life prediction method for lithium-ion battery based on long short-term memory network optimized by improved sparrow search algorithm," *Journal of Energy Storage*, vol. 61, May 2023.

[22] Y. Guo, P. Yu, and C. Zhu *et al*., "A state-of-health estimation method considering capacity recovery of lithium batteries," *International Journal of Energy Research*, vol. 46, no. 15, pp. 23730-23745, Dec. 2022.

[23] D. Li, D. Yang, and L. Li *et al*., "Electrochemical impedance spectroscopy based on the state of health estimation for lithium-ion batteries," *Energies*, vol. 15, no. 18, Sept. 2022.

[24] S. Cui, S. Riaz, and K. Wang, "Study on lifetime decline prediction of lithium-ion capacitors," *Energies*, vol. 16, no. 22, Nov. 2023.

[25] C. Zhang, C. Cao, and R. Chen *et al*., "Three-leg quasi-Z-source inverter with input ripple suppression for renewable energy application," *Energies*, vol. 16, no. 11, May 2023.

[26] W. Wang, D. Yang, and X. Yan *et al*., "Triboelectric nanogenerators: the beginning of blue dream," *Frontiers of Chemical Science and Engineering*, vol. 17, no. 6, pp. 635-678, Jun. 2023.

[27] W. Wang, D. Yang, and Z. Huang *et al*., "Electrodeless nanogenerator for dust recover," *Energy Technology*, vol. 10, no. 12, Oct. 2022.

[28] H. Zhang, J. Gao, and L. Kang *et al*., "State of health estimation of lithium-ion batteries based on modified flower pollination algorithm-temporal convolutional network," *Energy*, vol. 283, Nov. 2023.

[29] X. Sun, Y. Zhang, and Y. Zhang *et al*., "Summary of health-state estimation of lithium-ion batteries based on electrochemical impedance spectroscopy," *Energies*, vol. 16, no. 15, Aug. 2023.

[30] X. Yu, Y. Li, and X. Li *et al*., "Research on outdoor mobile music speaker battery management algorithm based on dynamic redundancy," *Technologies*, vol. 11, no. 2, Apr. 2023.

[31] X. Yu, Y. Shang, and L. Zheng *et al*., "Application of nanogenerators in the field of acoustics," *ACS Applied Electronic Materials*, vol. 5, no. 9, pp. 5240-5248, Sept. 2023.

[32] G. D. J. Harper, E. Kendrick, and P. A. Anderson *et al*., "Roadmap for a sustainable circular economy in lithium-ion and future battery technologies," *Journal of Physics-Energy*, vol. 5, no. 2, Apr. 2023.

[33] X. Qiu, W. Wu, and S. Wang, "Remaining useful life prediction of lithium-ion battery based on improved cuckoo search particle filter and a novel state of charge estimation method," *Journal of Power Sources*, vol. 450, Feb. 2020.

[34] Y. Li, B. Y. Xiong, and D. M. Vilathgamuwa *et al*., "Constrained ensemble kalman filter for distributed electrochemical state estimation of lithium-ion batteries," *IEEE Transactions on Industrial Informatics*, vol. 17, no. 1, pp. 240-250, Jan. 2021.

[35] A. El Mejdoubi, H. Chaoui, and J. Sabor *et al*., "Remaining useful life prognosis of supercapacitors under temperature and voltage aging conditions," *IEEE Transactions on Industrial Electronics*, vol. 65, no. 5, pp. 4357-4367, May 2018.

[36] Y. Ma, Y. Chen, and X. Zhou *et al*., "Remaining useful life prediction of lithium-ion battery based on gauss-hermite particle filter," *IEEE Transactions on Control Systems Technology*, vol. 27, no. 4, pp. 1788-1795, Jul. 2019.

[37] Z. Cui, L. Wang, and Q. Li *et al*., "A comprehensive review on the state of charge estimation for lithium-ion battery based on neural network," *International Journal of Energy Research*, vol. 46, no. 5, pp. 5423-5440, Apr. 2022.

[38] Q. Xia, X. Li, and K. Wang *et al*., "Unraveling the evolution of transition metals during Li alloying-dealloying by in-operando magnetometry," *Chemistry of Materials*, vol. 34, no. 13, pp. 5852-5859, Jun. 2022.

[39] S. Cui, S. Lyu, and Y. Ma, *et al*., "Improved Informer PV power short-term prediction model based on weather typing and AHA-VMD-MPE," *Energy*, vol. 307, Oct. 2024.

[40] W. Wang, D. Yang, and X. Yan *et al*., "Triboelectric nanogenerators: the beginning of blue dream," *Frontiers of Chemical Science and Engineering*, vol. 17, no. 6, pp. 635-678, Jun. 2023.

[41] T. Han, Z. Wang, and H. Meng, "End-to-end capacity estimation of Lithium-ion batteries with an enhanced long short-term memory network considering domain adaptation," *Journal of Power Sources*, vol. 2022, Feb. 2022.

[42] Z. Deng, X. Hu, and P. Li *et al*., "Data-driven battery state of health estimation based on random partial charging data," *IEEE Transactions on Power Electronics*, vol. 37, no. 5, pp. 5021-5031, May 2022.

[43] Y. Tan and G. Zhao, "Transfer learning with long short-term memory network for state-of-health prediction of lithium-ion batteries," *IEEE Transactions on Industrial Electronics*, vol. 67, no. 10, pp. 8723-8731, Oct. 2020.

[44] Z. Deng, L. Xu, and H. Liu *et al*., "Prognostics of battery capacity based on charging data and data-driven methods for on-road vehicles," *Applied Energy*, vol. 339, Jun. 2023.

[45] Y. Liu, G. Zhao, and X. Peng, "Deep learning prognostics for lithium-ion battery based on ensembled long short-term memory networks," *IEEE Access*, vol. 7, pp. 155130-155142, Aug. 2019.

[46] C. Liu, Y. Zhang, and J. Sun *et al*., "Stacked bidirectional LSTM RNN to evaluate the remaining useful life of supercapacitor," *International Journal of Energy Research*, vol. 46, no. 3, pp. 3034-3043, Oct. 2021.

[47] L. Ren, J. Dong, and X. Wang *et al*., "A data-driven Auto-CNN-LSTM prediction model for lithium-ion battery remaining useful life," *IEEE Transactions on Industrial Informatic*s, vol. 17, no. 5, pp. 3478-3487, Jul. 2021.

[48] Y. Dai and A. Yu, "Combined CNN-LSTM and GRU based health feature parameters for lithium-ion batteries SOH estimation," *Energy Storage Science and Technology*, vol. 11, no. 5, pp. 1641-1649, May 2022.

[49] Z. Xing, Y. He, and J. Chen *et al*., "Health evaluation of power transformer using deep learning neural network," *Electric Power Systems Research*, vol. 215, Feb. 2023.

[50] W. Wang, D. Yang, and Z. Huang *et al*., "Electrodeless nanogenerator for dust recover," *Energy Technology*, vol. 10, no. 12, Oct. 2022.

[51] Z. Alshingiti, R. Alaqel, and J. Al-Muhtadi *et al*., "A deep learning-based phishing detection system using CNN, LSTM, and LSTM-CNN," *Electronics*, vol. 12, no. 1, Jan. 2023.

[52] Z. He, J. Yang, and L. Yong, "A pharmacokinetic model based on the SSA-1DCNN-attention method," *Journal of Bioinformatics and Computational Biology*, vol. 21, no.1, Feb. 2023.

[53] D. Niu, M. Yu, and L. Sun *et al*., "Short-term multi-energy load forecasting for integrated energy systems based on CNN-BiGRU optimized by attention mechanism," *Applied Energy*, vol. 313, May 2022.

[54] G. I. Kim and B. Jang, "Petroleum price prediction with CNN-LSTM and CNN-GRU using skip-connection," *Mathematics*, vol. 11, no. 3, Jan. 2023.

[55] D. Paudel, A. De Wit, and H. Boogaard *et al*., "Interpretability of deep learning models for crop yield forecasting," *Computers and Electronics in Agriculture*, vol. 206, Mar. 2023.

[56] F. Aksan, Y. Li, and V. Suresh *et al*., "CNN-LSTM vs. LSTM-CNN to predict power flow direction: a case study of the high-voltage subnet of northeast germany," *Sensors*, vol. 23, no. 2, Jan. 2023.

[57] X. Du, W. Jia, and P. Yu *et al*., "RUL prediction based on GAM-CNN for rotating machinery," *Journal of the Brazilian Society of Mechanical Sciences and Engineering*, vol. 45, no. 3, Mar. 2023.

[58] P. Qin, H. Li, and Z. Li *et al*., "A CNN-LSTM car-following model considering generalization ability," *Sensors*, vol. 23, no. 2, Jan. 2023.

[59] M. Zhang, K. Wang, and Y. Zhou, "Online state of charge estimation of lithium-ion cells using particle filter-based hybrid filtering approach," *Complexity*, vol. 2020, Jan. 2020.

[60] Z. Cui, J. Dai, and J. Sun *et al*., "Hybrid methods using neural network and kalman filter for the state of charge estimation of lithium-ion battery," *Mathematical Problems in Engineering*, vol. 2022, May 2022.

[61] A. Graves and J. Schmidhuber, "Framewise phoneme classification with bidirectional LSTM and other neural network architectures," *Neural Networks*, vol. 18, no. 5, pp. 602-610, Jun. 2005.

[62] F. A. Hashim, E. H. Houssein, and K. Hussain *et al*., "Honey badger algorithm: new metaheuristic algorithm for solving optimization problems," *Mathematics and Computers in Simulation*, vol. 192, pp. 84-110, Feb. 2022.

[63] Y. Gal, "Uncertainty in deep learning," Ph.D. dissertation, the Department of Engineering, University of Cambridge, Cambridge, United Kingdom, 2016.